CHEMISTRY OF MATERIALS
Article

Chem. Mater. **2009,** *21,* 3503–3513 3503
DOI:10.1021/cm901329g

Defect Chemistry of a Zinc-Doped Lepidocrocite Titanate $Cs_xTi_{2-x/2}Zn_{x/2}O_4$ ($x = 0.7$) and its Protonic Form

Tao Gao,*[,†] Helmer Fjellvåg,[†] and Poul Norby[†,‡]

[†]*Centre for Materials Science and Nanotechnology and Department of Chemistry, University of Oslo, P.O. Box 1033, N-0315 Oslo, Norway, and* [‡]*Materials Research Division, Risø National Laboratory for Sustainable Energy, Technical University of Denmark, P.O. Box 49, DK-4000 Roskilde, Denmark*

Received May 14, 2009. Revised Manuscript Received June 23, 2009

A zinc-doped layered titanate $Cs_xTi_{2-x/2}Zn_{x/2}O_4$ ($x = 0.7$) with lepidocrocite (γ-FeOOH)-type layered structure was prepared via solid-state calcination. A complete extraction of both lattice Zn atoms and interlayer Cs ions was observed upon acid exchange, producing a protonic form $H_{2x}Ti_{2-x/2}\square_{x/2}O_4 \cdot H_2O$ that inherited the original lepidocrocite-type layered structure. This new phase was distinguished from its isomorphous related compounds in terms of high proton content, high charge density, and high defect content as a consequence of extractable Zn atoms located in the host framework. The protonic titanate $H_{2x}Ti_{2-x/2}\square_{x/2}O_4 \cdot H_2O$ readily underwent delamination to produce its molecular single sheets $Ti_{1-\delta}\square_\delta O_2^{4\delta-}$ ($\delta = 0.175$) with distinctive two-dimensional morphology and small thickness (~1 nm), suggesting promising applications in the assembly of functional nanostructures.

Introduction

Layered titanates with lepidocrocite (γ-FeOOH)-type layered structure (denoted as lepidocrocite titanates hereafter) represent a large class of isomorphous compounds that can be formulated as $A_xTi_{2-y}M_yO_4$,[1−5] where A is Cs, Rb, or K; x is reported as 0.7, 0.75, and 0.8 for Cs, Rb, and K, respectively; M is any of vacancy, Li, Mg, Zn, Cu, Co, Ni, Fe(III), Mn(III), Sc or Al;[1−10] y is correlated to x according to $x = y(4-n)$ with n being the oxidation state of the lower valence metal substitutions ($n < 4$; $n = 0$ for M = vacancy). Structurally, lepidocrocite titanates $A_xTi_{2-y}M_yO_4$ usually crystallize in an orthorhombic structure, consisting of two-dimensional (2D) corrugated layers of edge and corner sharing octahedra and interlayer alkaline ion A, which compensates for the negative charge that arises from the substitution of M for Ti,[1−9] as shown schematically in Figure 1.

A wide range of uses of lepidocrocite titanates, especially in the field of nanotechnology,[11] is due to their excellent capability to intercalate a large variety of inorganic and organic species and to delaminate into 2D molecular single sheets (i.e., titanate nanosheets) under controlled conditions.[7−9,12,13] These nanosheets have unique anisotropic properties[14] and are promising building blocks for the assembly of artificial nanoarchitectures, such as hybrid multilayer films,[15] and microporous materials with inorganic pillars.[16] Critical to the functionality of these nanoarchitectures are the size and stoichiometry of the titanate nanosheets;[11] therefore, the control of the lattice substitutions/dopants M in lepidocrocite titanates $A_xTi_{2-y}M_yO_4$ is expected to have a significant impact on progress.[10] However, defect chemistry concerning physicochemical properties of the lattice

*Corresponding author. E-mail: tao.gao@kjemi.uio.no.

(1) Reid, A. F.; Mumme, W. G.; Wadsley, A. D. *Acta Crystallogr., Sect. B* **1968**, *24*, 1228–1233.
(2) Birchall, T.; Greenwood, N. N.; Reid, A. F. *J. Chem. Soc., A* **1969**, *16*, 2382–2398.
(3) Verbaère, A.; Dion, M.; Tournoux, M. *Rev. Chim. Minér.* **1975**, *12*, 156–174.
(4) Groult, D.; Mercy, C.; Raveau, B. *J. Solid State Chem.* **1980**, *32*, 289–296.
(5) Hervieu, M.; Raveau, B. *Rev. Chim. Minér.* **1981**, *18*, 642–649.
(6) Grey, I. E.; Li, C.; Madsen, I. C.; Watts, J. A. *J. Solid State Chem.* **1987**, *66*, 7–19.
(7) England, W. A.; Birkett, J. E.; Goodenough, J. B.; Wiseman, P. J. *J. Solid State Chem.* **1983**, *49*, 300–308.
(8) Sasaki, T.; Kooli, F.; Iida, M.; Michiue, Y.; Takenouchi, S.; Yajima, Y.; Izumi, F.; Chakoumakos, B. C.; Watanabe, M. *Chem. Mater.* **1998**, *10*, 4123–4128.
(9) Gao, T.; Fjellvåg, H.; Norby, P. *J. Mater. Chem.* **2009**, *19*, 787–794.
(10) (a) Osada, M.; Ebina, Y.; Fukuda, K.; Ono, K.; Takada, K.; Yamaura, K.; Takayama-Muromachi, E.; Sasaki, T. Phys. Rev. B **2006**, *73*, 153301. (b) Osada, M.; Ebina, Y.; Takada, K.; Sasaki, T. *Adv. Mater.* **2006**, *18*, 295–299.(c) Osada, M.; Itose, M.; Ebina, Y.; Ono, K.; Ueda, S.; Kobayashi, K.; Sasaki, T. Appl. Phys. Lett. **2008**, *92*, 253110.
(11) (a) Sasaki, T. *J. Ceram. Soc. Jpn.* **2007**, *115*, 9–16. (b) Osada, M.; Sasaki, T. *J. Mater. Chem.* **2009**, *19*, 2503–2511.
(12) Suzuki, N.; Hayashi, N.; Honda, C.; Endo, K.; Kanzaki, Y. *Bull. Chem. Soc. Jpn.* **2006**, *79*, 711–716.
(13) (a) Sasaki, T.; Watanabe, M.; Hashizume, H.; Yamada, H.; Nakazawa, H. *J. Am. Chem. Soc.* **1996**, *118*, 8329–8335. (b) Sasaki, T.; Watanabe, M. *J. Am. Chem. Soc.* **1998**, *120*, 4682–4689.
(14) (a) Sakai, N.; Ebina, Y.; Takada, K.; Sasaki, T. *J. Am. Chem. Soc.* **2004**, *126*, 5851–5858. (b) Sasaki, T.; Watanabe, M. *J. Phys. Chem. B* **1997**, *101*, 10159–10161. (c) Sato, H.; Ono, K.; Sasaki, T.; Yamagishi, A. *J. Phys. Chem. B* **2003**, *107*, 9824–9828.
(15) (a) Zhou, Y.; Ma, R.; Ebina, Y.; Takada, K.; Sasaki, T. *Chem. Mater.* **2006**, *18*, 1235–1239. (b) Sasaki, T.; Ebina, Y.; Tanaka, T.; Harada, M.; Watanabe, M.; Decher, G. *Chem. Mater.* **2001**, *13*, 4661–4667. (c) Paek, S. M.; Jung, H.; Lee, Y. J.; Park, M.; Hwang, S. J.; Choy, J. H. *Chem. Mater.* **2006**, *18*, 1134–1140.
(16) (a) Choy, J. H.; Lee, H. C.; Jung, H.; Hwang, S. J. *J. Mater. Chem.* **2001**, *11*, 2232–2234. (b) Kim, T. W.; Hur, S. G.; Hwang, S. J.; Choy, J. H. *Chem. Commun.* **2006**, 220–222.

Published on Web 07/08/2009

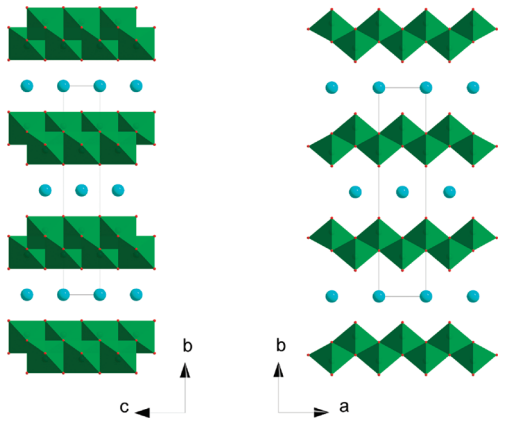

Figure 1. Polyhedral representation of the crystal structure for lepidocrocite titanates $A_xTi_{2-y}M_yO_4$. The low valence metal ion substitutions or vacancies in the octahedral host layers are not shown for simplification. Solid lines show the orthorhombic unit cell.

substitutions/dopants in lepidocrocite titanates has not been well- understood.

Most of the lattice substitutions/dopants in lepidocrocite titanates $A_xTi_{2-y}M_yO_4$ are immobile upon acid leaching,[10] whereas some of them are reported to be exchangeable.[8,9] For example, a complete extraction of both lattice Li atoms and interlayer alkali species was observed during the acid exchange of a Li-doped titanate $A_xTi_{2-x/3}Li_{x/3}O_4$ (A = K, Rb, and Cs),[8] producing a protonic from $H_{4x/3}Ti_{2-x/3}\square_{x/3}O_4\cdot H_2O$ (note that we prefer this formulation because it better represents its structural features than the original $H_{4x/3}Ti_{2-x/3}O_4\cdot H_2O$[8]). On the other hand, lattice dopants such as Co atoms in an isomorphous compound $K_xTi_{2-x/2}Co_{x/2}O_4$ were found to be stable upon acid exchange, forming a protonic titanate $H_xTi_{2-x/2}Co_{x/2}O_4\cdot H_2O$ that can be further delaminated into $Ti_{1-x/4}Co_{x/4}O_2$ nanosheets with interesting magnetic properties.[10] A complete extraction of lattice Mg atoms from an Mg-doped titanate $Cs_xTi_{2-x/2}Mg_{x/2}O_4$ ($x = 0.7$) was reported recently, bringing about a protonic form $H_xTi_{2-x/2}O_{4-x/2}\cdot H_2O$ that is notable for its reduced lattice oxygen contents.[9] So far, it is still not clear how and why these different physicochemical processes can be performed in lepidocrocite titanates with different lattice substitutions/dopants. For an improved understanding of the dopant-dependent physicochemical properties of lepidocrocite titanates,[8−10] we consider it interesting as well as important to discover new compositions with extractable lattice substitutions/dopants.

We report here the intriguing defect chemistry observed in a zinc-doped lepidocrocite titanate $Cs_xTi_{2-x/2}Zn_{x/2}O_4$ (x = 0.7), of which a complete extraction of both interlayer Cs ions and the lattice Zn atoms is achieved upon protonation, resulting in a new protonic titanate with composition $H_{2x}Ti_{2-x/2}\square_{x/2}O_4\cdot H_2O$. this new titanate shows several surprising structural features as a consequence of extractable lattice Zn atoms and interlayer Cs ions. For example, the titanate $H_{2x}Ti_{2-x/2}\square_{x/2}O_4\cdot H_2O$ has the highest proton content (1.4/unit for x=0.7) in comparison with its isomorphous related compounds such as $H_xTi_{2-x/4}\square_{x/4}O_4\cdot H_2O$ (0.7/unit for x=0.7)[17,18] and $H_{4x/3}Ti_{2-x/3}\square_{x/3}O_4\cdot H_2O$ (0.93/unit for x = 0.7).[8] Although the $H_{2x}Ti_{2-x/2}\square_{x/2}O_4\cdot H_2O$ is characteristic by the high defect content (i.e., the vacant octahedral sites in the host framework), its lepidocrocite-type layered structure is surprisingly stable in acidic solutions, which is in sharp difference from its isomorphous compound $H_xTi_{2-x/4}O_{4-x/2}\cdot H_2O$.[9] Furthermore, the $H_{2x}Ti_{2-x/2}\square_{x/2}O_4\cdot H_2O$ possesses excellent exchange capabilities to accommodate a variety of inorganic and organic cations in its interlay spaces, which seems unusual for a layered compound with an extraordinarily high charge density (0.060/Å^2, in comparison with 0.031/Å^2 observed for $H_xTi_{2-x/4}\square_{x/4}O_4\cdot H_2O$[17]).

Experimental Section

Reagents and Materials. All metal oxides and carbonates used in this work were of >99% purity or of analytical grade. Polyethylenimine (PEI, $M_w \approx 25\,000$), tetramethylammonium (TMA) hydroxide (10 wt % solution), and tetrabutylammonium (TBA) hydroxide (40 wt % solution) solution were purchased from Sigma-Aldrich Co. and used as received.

Zinc-doped titanate $Cs_xTi_{2-x/2}Zn_{x/2}O_4$ (x=0.7) was prepared by following the procedures for $Cs_xTi_{2-x/2}Mg_{x/2}O_4$ (x=0.7).[9] A mixture of Cs_2CO_3, ZnO, and TiO_2 with a molar ration of 1:1:4.7 was placed in an alumina crucible and heated in air at 800 °C for 30 min in order to remove carbonate. After cooling, the decarbonated powders were ground and subjected to two heat treatments (950 °C, 20 h) with intermediate grinding. For comparison, several isomorphous cesium-loaded titanates $Cs_xTi_{2-y}M_yO_4$ (x = 0.7, M = vacancy, Li, Mg, Cu, Co, and Ni) were also prepared.[6−9]

The protonic form of $Cs_xTi_{2-x/2}Zn_{x/2}O_4$ was obtained via acid exchange. For a typical reaction, 100 mg $Cs_xTi_{2-x/2}Zn_{x/2}O_4$ powder was dispersed in 100 mL of H_2SO_4 aqueous solution (1 M) at room temperature for 3 days. The acidic solution was renewed every day to promote a complete exchange. After the exchange reaction, the solid material was filtered, rinsed with water, and dried in air at room temperature. To explore the structural stability, we subsequently heated the as-prepared protonic titanate in air at different temperatures for 2.5 h.

Intercalation of organic amines was achieved by dispersing 50 mg of protonic titanate powder into 100 mL of amine (TMA^+OH^- and TBA^+OH^-) solutions (5 wt %). The intercalation reaction was carried out at 60 °C under constant stirring for 1 week. The solid product was thereafter separated from the suspension by centrifugation. A stable colloidal suspension was obtained by dispersing the solid product in water. Freeze−drying of the colloidal suspension yielded a voluminous cottonlike solid.

X-ray Photoelectron Spectroscopy (XPS). Around ~50 mg of the as-prepared materials were pressed into pellets and attached to the XPS sample holder via conductive carbon glue. XPS spectra were collected with a KRATOS Axis Ultra-DLD spectrometer using monochromatic Al Kα radiation (1486.6 eV). A pass energy of 80 eV with a step size of 1 eV was used for survey scans. For separate photoelectron lines, a pass energy of 20 eV was used with a step size of 0.1 eV. The surface of the sample was flooded with low-energy electrons to compensate for electrostatic charging. All samples were studied at a pressure of 3×10^{-9} Torr. During the analysis samples were frozen at −140 °C to preserve

(17) Sasaki, T.; Watanabe, M.; Michiue, Y.; Komatsu, Y.; Izumi, F.; Takenouchi, S. *Chem. Mater.* **1995**, *7*, 1001–1007.

(18) Gao, T.; Fjellvåg, H.; Norby, P. *J. Phys. Chem. B* **2008**, *112*, 9400–9405.

the interlayer water. Spectra were analyzed using CasaXPS software (version 1.0.0.1);[19] energy referencing was based on the C−C component of the C 1*s* photoelectron peak at 284.8 eV.

Vibrational Spectroscopy. Fourier Transform infrared (FT-IR) data were recorded for samples prepared via the standard KBr technique on a PerkinElmer Spectrum 2000 FT-IR spectrometer (resolution: ~2 cm^{-1}). Raman scattering spectra were collected at room temperature in a backscattering configuration; the samples were illuminated by using a 632.8 nm He−Ne laser on an Olympus BX 40 confocal microscope with a 50× objective. The wavenumber stability and the accuracy of the apparatus were calibrated by recording the F_{2g} Raman-active mode of silicon at 521 cm^{-1}.

Structural Refinement. Synchrotron XRD data were collected at the Swiss-Norwegian Beamline BM01B, at the European Synchrotron Radiation Facility (ESRF) in Grenoble, France. The synchrotron XRD data were measured between 1 and 40° in 2θ using a wavelength of $\lambda = 0.6998$ Å in transmission geometry. The synchrotron XRD data were analyzed by the Rietveld method with GSAS[20] using EXPGUI.[21] Starting atomic coordinates for Cs, Ti, Zn and O were taken from those reported for $Cs_xTi_{2-x/2}Mg_{x/2}O_4$ ($x = 0.7$).[9] Trace amounts of unknown impurities were noticed during the refinement, but it was not possible to identify the impurity phase or phases. In addition a broad peak was observed at 10−11° in 2θ. An excluded region around this peak was used in the refinements. The calculated intensity of the 110 reflection, which was situated in the excluded region, matched well with the observed intensity.

Characterization. The as-prepared materials were also characterized by powder X-ray diffraction (Siemens D5000 powder diffractometer; Cu Kα_1 radiation $\lambda = 1.540598$ Å) and scanning electron microscopy (SEM, FEI Quanta 200F) equipped with an energy-dispersive X-ray spectrometer (EDX). Chemical analysis was performed by LabNett AS, Norway; the samples were dissolved in a mixture of HF and H_2SO_4 aqueous solution and analyzed subsequently by inductively coupled plasma mass spectroscopy (ICP-MS). Thermogravimetric analysis (TGA) was performed on a Perkin-Elmer TGA 7 system in a nitrogen atmosphere at a heating rate of 10 °C min^{-1}. Atomic force microscope (AFM) images were collected on a Nanoscope E multimode AFM (Digital Instruments) in tapping mode; the silicon substrates used for depositing the nanosheets were pretreated with the PEI solution (5 g/L).

Results and Discussion

Crystal Structure of $Cs_xTi_{2-x/2}Zn_{x/2}O_4$. As indicated by the compositional formula $A_xTi_{2-y}M_yO_4$, lepidocrocite titanates are typical nonstoichiometric compounds. Previous studies suggested the presence of "magic numbers" for lepidocrocite titanate $A_xTi_{2-y}M_yO_4$ with $x = 0.7$, 0.75, and 0.8 for A = Cs, Rb, and K, respectively.[1−10] According to the charge compensation scheme, the compositional parameters x and y of the $A_xTi_{2-y}M_yO_4$ are correlated with each other according to $x = y(4 - n)$, with n being the oxidation state of the lower valence metal dopants ($n = 0$ for M = vacancy). This indicates that the compositional range for homogeneity of the lepidocrocite titanates $A_xTi_{2-y}M_yO_4$ is somewhat narrow; consequently, controlling the nature of lattice dopants M will be the most important approach to modify the structures and properties.[10]

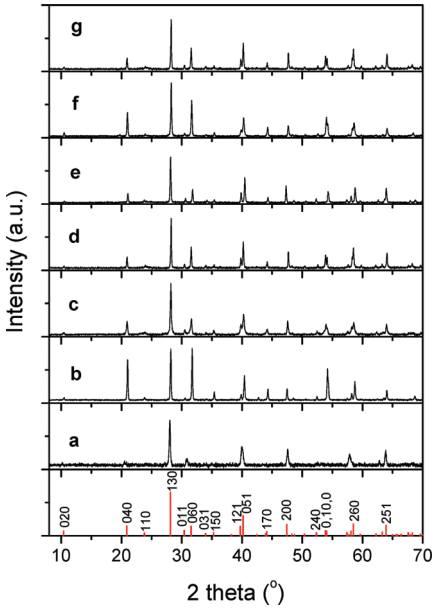

Figure 2. Powder XRD data for lepidocrocite titanates $Cs_xTi_{2-y}M_yO_4$ ($x = 0.7$), where M is vacancy, Li, Mg, Zn, Ni, Cu, and Co for pattern a, b, c, d, e, f, and g, respectively. Bars shown at the bottom are calculated from a body-centered orthorhombic structure (space group I*mmm*). Wavelength: 1.540598 Å.

A series of cesium-loaded titanates with mean composition $Cs_xTi_{2-y}M_yO_4$ ($x = 0.7$, M = vacancy, Li, Zn, Ni, Cu, and Co) can be readily synthesized, of which the powder XRD patterns of the as-synthesized materials are reported in Figure 2. Table 1 summarizes the calculated lattice parameters for comparison. Apparently, these compounds are structurally equivalent, as demonstrated by their similar XRD reflection positions. The as-prepared materials can be indexed on the basis of a body-centered orthorhombic structure (space group *Immm*) with slightly different unit cell dimensions (Table 1). The variation of lattice parameters of the $Cs_xTi_{2-y}M_yO_4$ may possibly correlate with the different radii[22] or electronegativity[23] of the involved lattice dopants (Table 1). The results reveal that, one the one hand, the symmetry of the lepidocrocite titanate $A_xTi_{2-y}M_yO_4$ are correlated mainly with the interlayer cation A, regardless of the nature of the lattice dopants M;[1,4,6] one the other hand, the replacement or mixing of these different lattice dopants will result in the formation of a considerable number of isomorphous compounds with intermediate compositions.[1,2] Preliminary synthesis indicates that lepidocrocite titanates $Cs_xTi_{2-x/2}(M_yN_{1-y})_{x/2}O_4$ ($x = 0.7$; $0 \le y \le 1$; M and N are any two of Ni, Zn, Mg, Cu, and Co) can be readily synthesized, showing the possibility to study the dopant-dependent structural and physical properties.[24]

Rietveld analysis was performed with the Zn-doped phase $Cs_xTi_{2-x/2}Zn_{x/2}O_4$ to get information on a precise

(19) http://www.casaxps.com
(20) Larson, A. C.; Von Dreele, R. B. General Structure Analysis System; Los Alamos National Laboratory Report LAUR 86-748; Los Alamos National Laboratory: Los Alamos, NM, **1994**.
(21) Toby, B. H. *J. Appl. Crystallogr.* **2001**, *34*, 210–213.
(22) Shannon, R. D.; Prewitt, C. T. *Acta Crystallogr.* **1969**, *B25*, 925–946.
(23) Huheey, J. E. Inorganic Chemistry: Principles of Structure and Reactivity, 3rd ed.; Harper & Row: New York, 1983.
(24) Gao, T.; Fjellvåg, H.; Norby, P. Unpublished data.

Table 1. Lattice Parameters for Cesium Titanates $Cs_xTi_{2-y}M_yO_4$; Calculated Standard Deviations are in Parentheses

compd	x	a (Å)	b (Å)	c (Å)	V (Å^3)	r_M (Å)[a]	X_M[b]
$Cs_xTi_{2-x/2}Cu_{x/2}O_4$	0.68	3.7946(1)	16.8945(4)	2.9647(1)	190.06(1)	0.730	2.00
$Cs_xTi_{2-x/2}Ni_{x/2}O_4$	0.67	3.8420(1)	16.9050(3)	2.9666(1)	192.68(1)	0.700	1.91
$Cs_xTi_{2-x/2}Co_{x/2}O_4$	0.70	3.8296(1)	16.9581(5)	2.9792(1)	193.48(1)	0.735	1.88
$Cs_xTi_{2-x/2}Zn_{x/2}O_4$	0.68	3.8143(1)	17.0205(4)	2.9837(1)	193.71(1)	0.745	1.65
$Cs_xTi_{2-x/2}Mg_{x/2}O_4$[c]	0.64	3.8283(0)	17.0064(1)	2.9814(0)	194.11(0)	0.720	1.31
$Cs_xTi_{2-x/3}Li_{x/3}O_4$[d]	0.64	3.8298(1)	16.9340(3)	2.9712(1)	192.69(1)	0.740	0.98
$Cs_xTi_{2-x/4}\square_{x/4}O_4$[e,f]	0.68	3.8433(1)	17.1520(6)	2.9601(1)	195.13(1)	-	-

[a] Effective radii of M according to ref [22] (coordinated oxygen number: 6). [b] Pauling electronegativity of M according to ref [23]. [c] According to ref [9] and shown here for composition. [d] From ref [8]: $x = 0.7$, $a = 3.8326(2)$ Å, $b = 16.9245(8)$ Å, and $c = 2.9731(1)$ Å. [e] From ref [17]: $x = 0.7$, $a = 3.837(1)$ Å, $b = 17.198(3)$ Å, and $c = 2.960(1)$ Å. [f] From ref [6]: $0.61 < x < 0.65$, $a = 3.831(3)$ Å, $b = 17.021(18)$ Å, and $c = 2.964(3)$ Å.

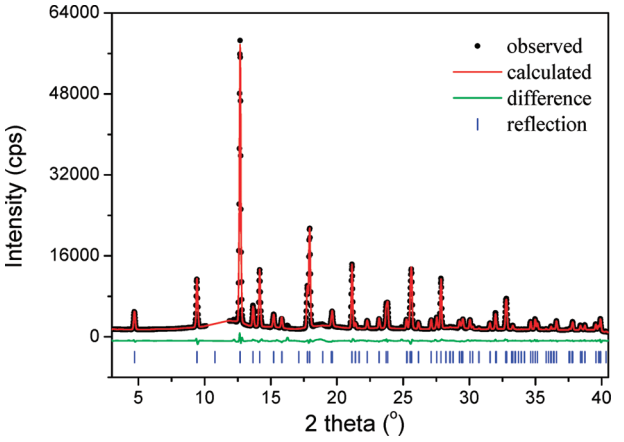

Figure 3. Final results of the Rietveld fitting of synchrotron X-ray diffraction data for $Cs_xTi_{2-x/2}Zn_{x/2}O_4$ ($x = 0.7$) The data region from 10.1 to 11.8° was excluded during the refinement because of a broad bump. Wavelength: 0.6998 Å.

accommodation manner of the lattice dopants and interlayer cations. The observed, calculated and difference profiles are illustrated in Figure 3. Atomic coordinates and displacement parameters are given in Table 2. Selected interatomic distances are reported in Table 3. The final refinement on the basis of the body-centered orthorhombic structure (space group *Immm*) yields a satisfactory convergence with the residual indices of $R_{wp} = 0.037$ and $R_p = 0.026$. The refined unit-cell dimensions are $a = 3.81426(7)$ Å, $b = 17.0205(4)$ Å, and $c = 2.98373(6)$ Å (see Table 1). This gives an interlayer distance of about 8.51 Å, which is a typical value seen for other isomorphous compounds such as $Cs_xTi_{2-x/4}\square_{x/4}O_4$ ($d = 8.57$ Å),[6,17] $Cs_xTi_{2-x/3}Li_{x/3}O_4$ ($d = 8.47$ Å),[8] and $Cs_xTi_{2-x/2}Mg_{x/2}O_4$ ($d = 8.50$ Å).[7,9]

The Rietveld refinements require anisotropic displacement parameters for the interlayer Cs atoms (Table 2). Significant improvement in the refinement has been achieved by introducing anisotropic displacement parameters for Cs atoms while applying isotropic displacement parameters for the rest. Moreover, a splitting of Cs position into 4*i*, (0,0,*z*) and (0,0,−*z*), is necessary to attain a good fit (Table 2). Analogous splitting of interlayer Cs ions has been suggested previously in isomorphous compounds, such as $Cs_xTi_{2-x/4}\square_{x/4}O_4$[6,17] and $Cs_xTi_{2-x/2}Mg_{x/2}O_4$.[9] The refinement shows a large elongation of the ellipsoid along the *c*-axis, indicating static or dynamic disorder on the Cs positions. This is in line with the partial occupancy ($x \approx 0.68$) by Cs of the available interlayer sites. The refinement concludes that the lattice Zn atoms occupy the

Table 2. Atomic Coordinates and Equivalent Isotropic Displacement Parameters (Å^2) for $Cs_xTi_{2-x/2}Zn_{x/2}O_4$. Calculated Standard Deviations are in Parentheses

atom	position	population	x	y	z	U_{iso}
Cs	4*i*	0.34	0	0	0.1628(6)	0.0552[b]
M[a]	4*h*	1	0	0.3121(1)	0.5	0.010(1)
O1	4*g*	1	0	0.2201(2)	0	0.023(1)
O2	4*g*	1	0	0.3758(2)	0	0.016 (1)

[a] Virtual species of ($0.825Ti^{4+} + 0.175Zn^{2+}$). [b] $U_{11} = 0.024(1)$, $U_{22} = 0.017(1)$, $U_{33} = 0.125(3)$, $U_{12} = U_{13} = U_{23} = 0$.

Table 3. Selected Interatomic Distances (Å) in $Cs_xTi_{2-x/2}Zn_{x/2}O_4$; Calculated Standard Deviations are in Parentheses

atoms	distance (Å)	atoms	distance (Å)
M[a]−O1	1.845(2) × 2	Cs−O1	3.019(3) × 4
M−O2	1.984(1) × 2	Cs−O1	3.466(2) × 4
M−O2	2.162(2) × 2	Cs−O2	3.778(3) × 2

[a] Virtual species of ($0.825Ti^{4+} + 0.175Zn^{2+}$).

octahedral sites in the 2D corrugated host layers and the Cs ions take the interlayer positions. Substitution Zn^{2+} for Ti^{4+} in the nominal TiO_2 framework results in negative charge that is balanced by the interlayer Cs^+ ions. The charge compensation scheme is the same as those reported for $Cs_xTi_{2-x/4}\square_{x/4}O_4$,[6] $A_xTi_{2-x/3}Li_{x/3}O_4$ (A = K, Rb, and Cs),[8] and $Cs_xTi_{2-x/2}Mg_{x/2}O_4$.[7,9]

The crystal structure of $Cs_xTi_{2-x/2}Zn_{x/2}O_4$ indicates the presence of both 4- and 2-coordinated anions, O2 and O1 (Table 2), in the 2D TiO_6 octahedral host layers; both sites are occupied by oxygen.[1,6] This results in the formal valence sum 2.67 and 1.33 for O2 and O1, respectively.[6] The sites are thus severely over- and undersaturated, respectively. The (Ti/Zn)O_6 octahedron in the framework are much distorted, characterizing for two long Ti/Zn−O2 bonds 2.162(2) Å and two short Ti/Zn−O1 bonds 1.845(2) Å. The Ti/Zn atoms are located off-centered toward the O1−O1 edges (e.g., Figure 1). The interlayer Cs ions are located off-centered within a rectangular prism of eight O1 atoms, four from one layer and four from the next (e.g., Figure 1). This gives four long Cs−O1 bonds, 3.466(2) Å and four short Cs−O1 bonds, 3.019(3) Å; there are two additional 4-coordinated O2 atoms further away at 3.778(3) Å, which are probably unbonded. Note that only 70% of the interlayer sites are occupied randomly by the Cs^+ ions and the rest are vacancies.

Protonation of $Cs_xTi_{2-x/2}Zn_{x/2}O_4$. The protonic form of $Cs_xTi_{2-x/2}Zn_{x/2}O_4$ was obtained by acid exchange. As shown in Figure 4, the resulting protonic titanate can be

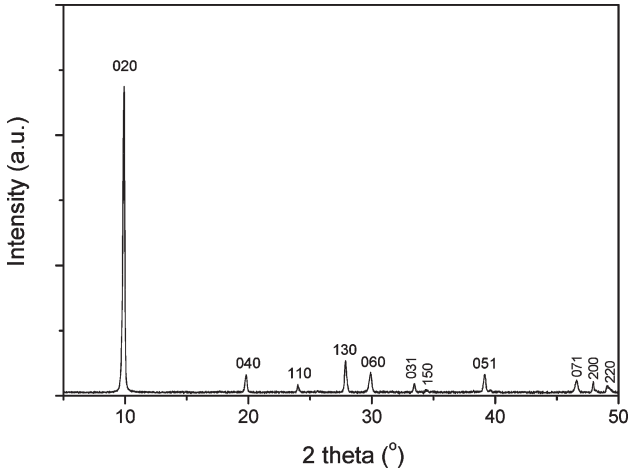

Figure 4. Powder XRD pattern of the protonic form of $Cs_xTi_{2-x/2}Zn_{x/2}O_4$ ($x = 0.7$). Wavelength: 1.540598 Å.

indexed to an orthorhombic structure (space group I*mmm*) with unit cell dimensions $a = 3.7953(3)$ Å, $b = 17.9389(4)$ Å, and $c = 3.0692(5)$ Å, isomorphous to the $H_xTi_{2-x/4}\square_{x/4}O_4 \cdot H_2O$,[17] the $H_{4x/3}Ti_{2-x/3}\square_{x/3}O_4 \cdot H_2O$,[8] and the $H_xTi_{2-x/2}O_{4-x/2} \cdot H_2O$.[9] It indicates that the lepidocrocite-type layered structure of the $Cs_xTi_{2-x/2}Zn_{x/2}O_4$ is preserved throughout during the acid exchange. According to the XRD data, the calculated interlayer distance of the resulting protonic titanate is about 8.97 Å, which is larger than that for the original $Cs_xTi_{2-x/2}Zn_{x/2}O_4$, 8.51 Å. This reveals that the interlayer Cs ions in the parent titanate have been exchanged with protons, probably in forms of H_3O^+, similar to those observed for the $Cs_xTi_{2-x/4}\square_{x/4}O_4$,[17,18] $A_xTi_{2-x/3}Li_{x/3}O_4$ (A=K, Rb, and Cs),[8] and $Cs_xTi_{2-x/2}Mg_{x/2}O_4$.[7,9] The presence of the interlayer water molecules was confirmed by the subsequent structural characterization.

It is found that the obtained protonic titanate is very stable under acidic solutions; no obvious structural degradations can be observed as the acid exchange reaction is prolonged up to 5 days (Figure 5). This is remarkably different from that seen for the $Cs_xTi_{2-x/2}Mg_{x/2}O_4$, which is gradually dissolved upon acid exchange.[7,9] It suggests the protonation of the $Cs_xTi_{2-x/2}Zn_{x/2}O_4$ in this work would yield different products than $H_xTi_{2-x/2}O_{4-x/2} \cdot H_2O$, the protonic form of the $Cs_xTi_{2-x/2}Mg_{x/2}O_4$.[9] The compositional evolution during the acid exchange of the $Cs_xTi_{2-x/2}Zn_{x/2}O_4$ was therefore examined. It is found that both the Zn atoms in the host frameworks and interlayer Cs ions are extractable, similar to those observed in the $A_xTi_{2-x/3}Li_{x/3}O_4$[8] and the $Cs_xTi_{2-x/2}Mg_{x/2}O_4$.[9] According to the ICP-MS data (Table 4), about 99.8% and 88.4% extraction of the Cs and Zn ions, respectively, was achieved after three cycles of acid exchange. A complete extraction of both the Cs and the Zn ions has been achieved after five cycles of acid exchange, as demonstrated by the EDX spectra, Figure 6.

Structure of $H_{2x}Ti_{2-x/2}\square_{x/2}O_4 \cdot H_2O$. Thanks to the charge compensation scheme, every Zn atoms will be exchanged with two protons. This brings about an interesting as well as important question: how will these exchanged protons be accommodated in the resulting

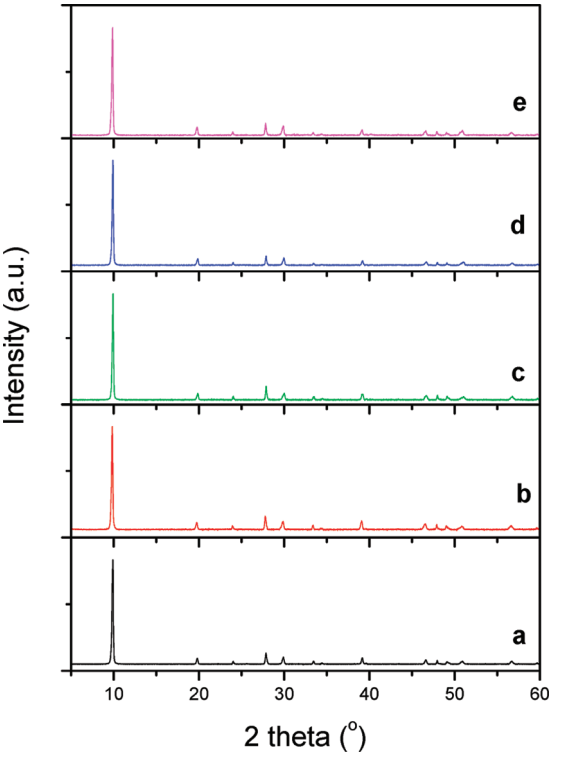

Figure 5. (color online) Powder XRD patterns for lepidocrocite titanate $Cs_xTi_{2-x/2}Zn_{x/2}O_4$ ($x = 0.7$) after acid exchange for (a) 1, (b) 2, (c) 3, (d) 4, and (e) 5 days, respectively. Wavelength: 1.540598 Å.

Table 4. Chemical Analysis Data for $Cs_xTi_{2-x/2}Zn_{x/2}O_4$ and its Protonic Form after 3-Day Acid Exchange

compound	Cs (mg/kg)	Zn (mg/kg)	Ti (mg/kg)	Cs/Ti (molar ratio)	Zn/Ti (molar ratio)
cesium form	387256	97769	293767	0.47	0.24
protonic form	1731	19771	510411	0.001	0.028

protonic titanate? These protons can be either located at the octahedral sites that originally occupied by the Zn atoms or accommodated in the interlayer regions. Inspired by the previous studies on isomorphous compounds such as $A_xTi_{2-x/3}Li_{x/3}O_4$ (A = K, Rb, and Cs)[8] and the $Cs_xTi_{2-x/2}Mg_{x/2}O_4$,[9] we suggest that the later were much probable. This has been confirmed by vibrational spectroscopic methods that are sensitive to local structural properties of materials.[18,25]

As reported in Figure 7, the protonic form of the $Cs_xTi_{2-x/2}Zn_{x/2}O_4$ shows similar vibrational features that are almost identical to those of the $H_xTi_{2-x/4}\square_{x/4}O_4 \cdot H_2O$[17,18] and the $H_{4x/3}Ti_{2-x/3}\square_{x/3}O_4 \cdot H_2O$,[8,25] demonstrating their similar local structural properties. One can immediately conclude that, on the one hand, the lattice Zn dopants are indeed extracted from the host framework of the $Cs_xTi_{2-x/2}Zn_{x/2}O_4$;[9] on the other hand, the extraction of the Zn atoms from the titanate will leave behind vacant octahedral sites within the 2D corrugated octahedral host layers. Previous studies on vibrational properties of isomorphous protonic titanates have demonstrated that

(25) Gao, T.; Fjellvåg, H.; Norby, P. The MRS International Materials Research Conference, Chongqing, China; Materials Research Society: Warrendale, PA, 2008; p 216.

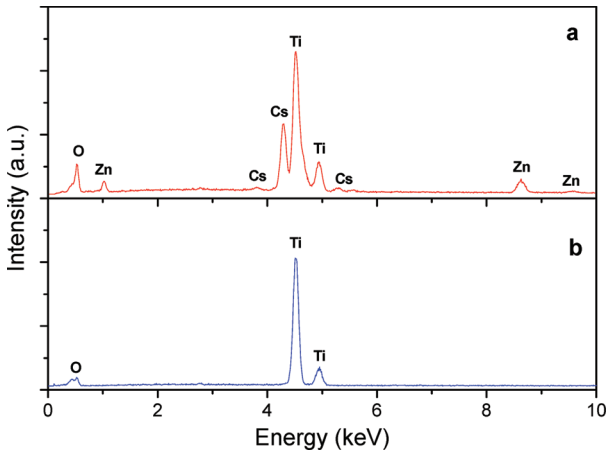

Figure 6. EDX spectra of (a) $Cs_xTi_{2-x/2}Zn_{x/2}O_4$ and (b) its protonic form after 5-day acid exchange.

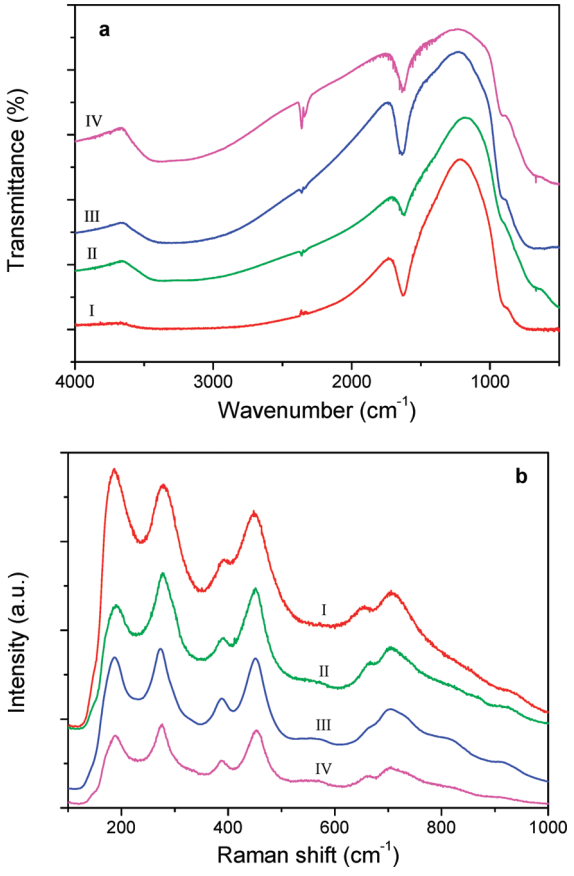

Figure 7. (a) FT-IR and (b) Raman scattering spectra of the protonic form of (I) $Cs_xTi_{2-x/2}Zn_{x/2}O_4$, (II) $Cs_xTi_{2-x/2}Mg_{x/2}O_4$, (III) $Cs_xTi_{2-x/4}\square_{x/4}O_4$, and (IV) $Cs_xTi_{2-x/3}Li_{x/3}O_4$. The curves II−IV are shown only for comparison and shifted vertically for clarity.

no protons would bond to the 2-coordinated oxygen atoms to form isolated hydroxyls in the interlayer regions.[8,9,17] It can thus be concluded from Figure 7 that the protonic form of the $Cs_xTi_{2-x/2}Zn_{x/2}O_4$ in this work only has protons in the form of H_3O^+ accommodated in the interlayer region.

As indicated by the TGA data, Figure 8a, the high-temperature phase $Cs_xTi_{2-x/2}Zn_{x/2}O_4$ does not show obvious weight loss (<0.2%) upon heating, indicating the surface absorbed water is neglectable, despite the presence of larger, vacant interlayer sites. In contrast,

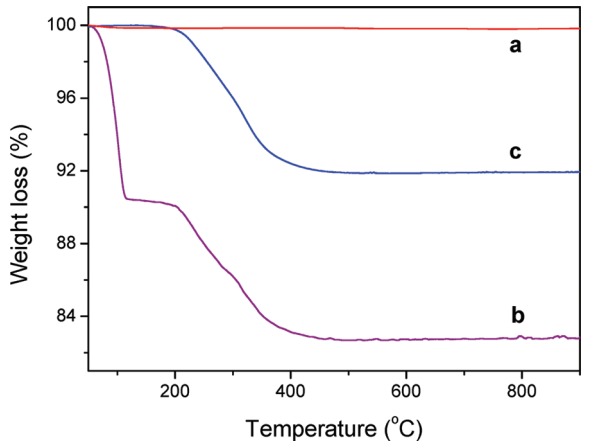

Figure 8. TGA curve of (a) $Cs_xTi_{2-x/2}Zn_{x/2}O_4$, (b) the resulting protonic titanate, and (c) the protonic titanate heated in air at 120 °C for 2.5 h.

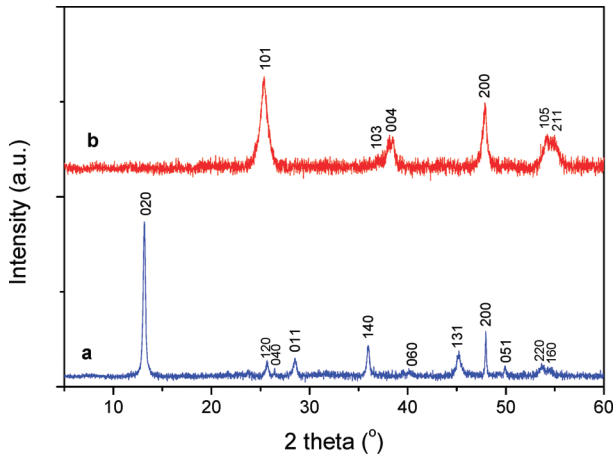

Figure 9. Powder XRD patterns of (a) dehydrated titanate and (b) anatase. XRD samples are prepared by heating the resulting protonic titanate at 120 °C (for a) or 450 °C (for b) in air. Curves are shifted vertically for clarity. Wavelength: 1.540598 Å.

the resulting protonic titanate (Figure 8b) shows two distinguished weight loss regions upon heating, 40−120 and 200−450 °C, with corresponding weight losses of about 9 and 8%, respectively. The XRD data (Figure 9a) of an intermediate at 120 °C indicated that the crystalline structure of the protonic titanate is degraded, with a contracted interlayer distance of about 0.67 nm, which is close to that of the lepidocrocite FeOOH without interlayer guests.[26] Thermal analyses on the intermediate at 120 °C (Figure 8c) give only one weight loss region, 200−450 °C, with corresponding weight loss of about 8%. These structural data suggest that, upon heating, the protonic titanate lost first interlayer water molecules, resulting in a dehydrated phase; that upon further heating undergoes complete dehydration to form the final anatase (Figure 9b).

There are so far three different protonation schemes for lepidocrocite titanates. The most common approach involves a direct exchange reaction between interlayer alkali ions and protons. For example, acid exchange of the $Cs_xTi_{2-x/4}\square_{x/4}O_4$ brings about the protonic form

(26) Ewing, F. J. *J. Chem. Phys.* **1935**, *3*, 420–424.

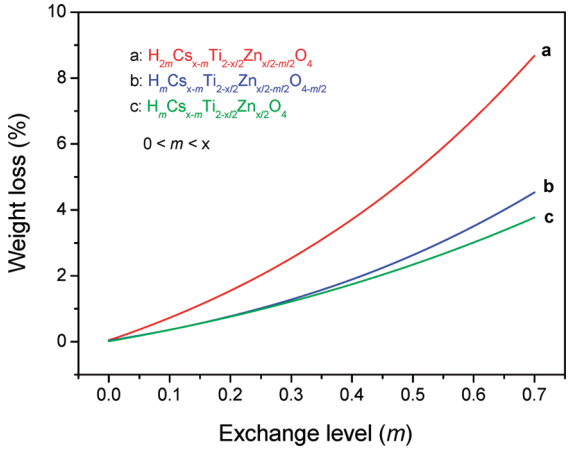

Figure 10. Expected weight loss of dehydrated protonic titanates upon the formation of final oxides. Three possible protonic forms of $Cs_xTi_{2-x/2}Zn_{x/2}O_4$ ($x = 0.7$) are considered for comparison.

$H_xTi_{2-x/4}\square_{x/4}O_4 \cdot H_2O$.[13,17,18] The Co-doped titanate $K_xTi_{2-x/2}Co_{x/2}O_4$ ($x = 0.8$) apparently follows the same exchange scheme.[10] Thanks to the extractable Zn atoms, this protonation scheme is not applicable for the $Cs_xTi_{2-x/2}Zn_{x/2}O_4$ in this work. Another protonation process has been proposed by Sasaki et al. for the mixed alkali metal titanate $A_xTi_{2-x/3}Li_{x/3}O_4$ (A = K, Rb, and Cs),[8] where the lattice Li atoms and the interlayer alkali ion A are extractable. This results in a protonic titanate $H_{4x/3}Ti_{2-x/3}\square_{x/3}O_4 \cdot H_2O$.[8] We have recently developed an improved model, $H_xTi_{2-x/2}O_{4-x/2} \cdot H_2O$, as the protonic form of the $Cs_xTi_{2-x/2}Mg_{x/2}O_4$ with extractable lattice Mg and O atoms.[9] Generally, these different protonation schemes will result in different proton contents of the 2D octahedral host layers, which can be conveniently examined by the corresponding weight losses of the dehydrated forms upon transformation of final oxides, Figure 10.

A larger weight loss upon heating would be achieved if the protonic form of the $Cs_xTi_{2-x/2}Zn_{x/2}O_4$ is $H_{2x}Ti_{2-x/2}\square_{x/2}O_4 \cdot yH_2O$. This corresponds to about 8.6% weight loss for the transformation of $H_{2x}Ti_{2-x/2}\square_{x/2}O_4$ to anatase (Figure 10a). It is in good agreement with the experimental value, ~8%. On the other hand, about 4.5 or 3.8% weight loss would be obtained, respectively, for the transformation of $H_xTi_{2-x/2}O_{4-x/2}$ or $H_xTi_{2-x/2}Zn_{x/2}O_4$ to final oxides (e.g., Figure 10b and 10c). In this regard, we conclude that the protonic form of the $Cs_xTi_{2-x/2}Zn_{x/2}O_4$ in this work is $H_{2x}Ti_{2-x/2}\square_{x/2}O_4 \cdot yH_2O$, where y is approximately 1 according to ~ 9% weight loss corresponding to the interlayer free water molecules (Figure 8b). In the following sections of this paper, the formulation $H_{2x}Ti_{2-x/2}\square_{x/2}O_4 \cdot H_2O$ will be used to represent the protonic form of the $Cs_xTi_{2-x/2}Zn_{x/2}O_4$.

Defects of $H_{2x}Ti_{2-x/2}\square_{x/2}O_4 \cdot H_2O$. It is worth pointing out that because the exchanged protons do not occupy the octahedral sites that originally located by the lattice Zn atoms, the protonic titanate $H_{2x}Ti_{2-x/2}\square_{x/2}O_4 \cdot H_2O$ will possess a large amount of defects, i.e., the vacant octahedral sites in the 2D host layers. The defect content of the $H_{2x}Ti_{2-x/2}\square_{x/2}O_4 \cdot H_2O$ would roughly be twice as high as that of the $H_xTi_{2-x/4}\square_{x/4}O_4 \cdot H_2O$.[13,17] Note that the

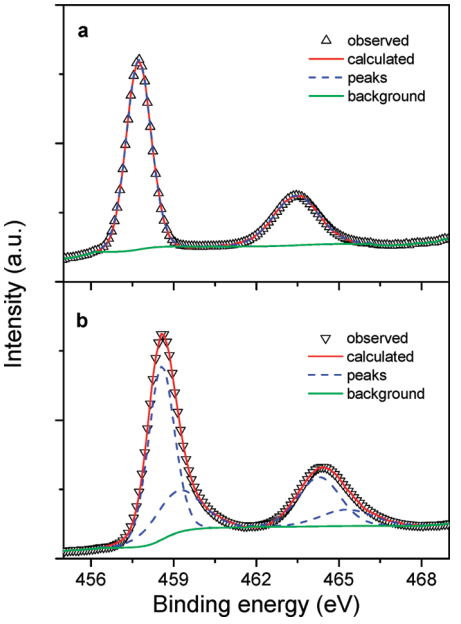

Figure 11. Ti 2p XPS spectra of (a) $Cs_xTi_{2-x/2}Zn_{x/2}O_4$ and (b) $H_{2x}Ti_{2-x/2}\square_{x/2}O_4 \cdot H_2O$.

removal of Zn atoms from the framework will bring about a deformation of their coordinated oxygen ligands in the $H_xTi_{2-x/4}\square_{x/4}O_4 \cdot H_2O$. Surprisingly, the protonic titanate $H_{2x}Ti_{2-x/2}\square_{x/2}O_4 \cdot H_2O$ still possesses almost identical local structural properties as those of the $H_xTi_{2-x/4}\square_{x/4}O_4 \cdot H_2O$ (e.g., Figure 7).[18,25] How the Ti site vacancies would be located in the 2D octahedral host layers would be an interesting question and worth studying. It shall be emphasized that, although the crystal structure for the $Cs_xTi_{2-x/4}\square_{x/4}O_4$ ($x = 0.7$) has been well-established,[6,17] it so far remains how the presence of vacant octahedral sites (i.e., Ti vacancies)[5,6] affect the distribution of oxygen ligands in the 2D host layers.

XPS was therefore employed in this work to shed lights on these defect-induced modifications. The wide-scan XPS spectrum of the $Cs_xTi_{2-x/2}Zn_{x/2}O_4$ shows the Ti, Cs, Zn, O, and C peaks, of which the C is due to the surface contamination. The Cs and Zn peaks disappear after the acid exchange reaction, wherea some interesting spectral modifications are observed in the Ti 2p and O 1s region, as shown in Figures 11 and 12, respectively. The peak parameters obtained by spectral fitting are listed in Tabled 5 and 6 for comparison.

As shown in Figure 11a, the Ti 2p XPS spectrum of the $Cs_xTi_{2-x/2}Zn_{x/2}O_4$ exhibits symmetrical profiles, indicating clearly a single oxidation state of the Ti atoms in the titanate.[27] There are two Ti 2p components with binding energy 457.7 eV for Ti $2p_{3/2}$ and 463.4 eV for Ti $2p_{1/2}$ (Table 5). Note that these values are about 1 eV lower than those observed for anatase single crystals, with Ti $2p_{3/2}$ and Ti $2p_{1/2}$ being 458.72 and 464.40 eV, respectively.[27a] We believe that the Ti atoms in the $Cs_xTi_{2-x/2}Zn_{x/2}O_4$ is still

(27) (a) Sanjinés, R.; Tang, H.; Berger, H.; Gozzo, F.; Margaritondo, G.; Lévy, F. *J. Appl. Phys.* **1994**, *75*, 2945–2951. (b) Kurtz, R. L.; Henrich, V. E. *Surf. Sci. Spectra* **1998**, *5*, 179–181. (c) Diebold, U.; Madey, T. E. *Surf. Sci. Spectra* **1998**, *4*, 227–231.

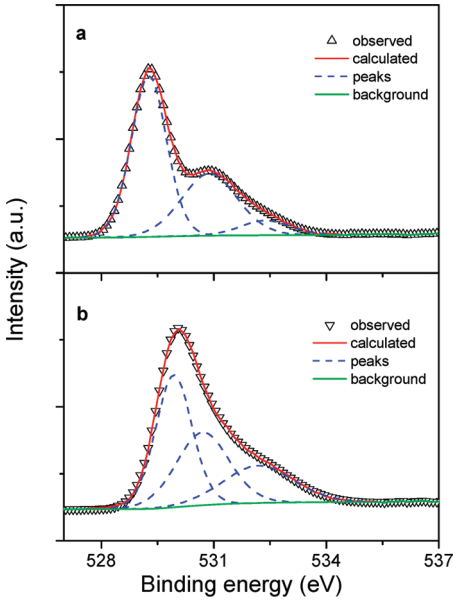

Figure 12. O 1s XPS spectra of (a) $Cs_xTi_{2-x/2}Zn_{x/2}O_4$ and (b) $H_{2x}Ti_{2-x/2}\square_{x/2}O_4\cdot H_2O$.

tetravalent because the existence of Ti^{3+} ions in the samples is very unlikely. For example, the $Cs_xTi_{2-x/2}Zn_{x/2}O_4$ is synthesized in air at high temperature (i.e., 950 °C) for a long time (i.e., 40 h), no reduction reactions can thus be expected and the oxidation state of the Ti atoms shall be the same as that of the TiO_2 precursors. Moreover, the presence of Ti^{3+} ions is not consistent with the structural studies (Figure 3 and Table 2). It shall be emphasized that the energy separation between the Ti $2p_{3/2}$ and Ti $2p_{1/2}$ is about 5.7 eV in this work, matching fairly well with those of the TiO_2 single crystals, 5.68 eV,[27] within the experimental error.

After the acid exchange reaction, the Ti 2p peaks of the resulting protonic titanate $H_{2x}Ti_{2-x/2}\square_{x/2}O_4\cdot H_2O$ are found to shift to the high binding energy side (Figure 11b). For example, the Ti $2p_{3/2}$ peak shifts from 457.7 to 458.5 eV (Table 5). Higher binding energies typically, but not always, denote a chemical state more oxidic in nature. Because the possibility of Ti^{5+} atoms being present in the protonic titanate is very small,[28] the binding energy shift to the high binding energy side may indicate that the interaction between the Ti atoms and the coordinated oxygens changes from week for the $Cs_xTi_{2-x/2}Zn_{x/2}O_4$ to strong for the $H_{2x}Ti_{2-x/2}\square_{x/2}O_4\cdot H_2O$. This seems in harmony with the Ti−O binding nature changes from Ti−O1−Cs to Ti−O1−H during the protonation.[24]

Moreover, as shown in Figure 11b, the total Ti $2p_{3/2}$ spectra can be fitted by introducing an additional Ti $2p_{3/2}$ component at higher binding energy situated at 459.1 eV with fwhm of about 2.0 eV (Table 5). Similarly, for the Ti $2p_{1/2}$ spectra, an additional Ti $2p_{1/2}$ component at 465.2 eV with fwhm of about 2.2 eV is also appeared, apart from the main peak at 464.2 eV (Figure 11b, Table 5). This new Ti 2p component with higher binding energy may be accounted for the presence of strong Ti−O interactions in

Table 5. Ti 2p Binding Energy and Energy Separation for $Cs_xTi_{2-x/2}Zn_{x/2}O_4$ and $H_{2x}Ti_{2-x/2}\square_{x/2}O_4\cdot H_2O$

compd	$2p_{3/2}$ (eV)[a]	$2p_{1/2}$ (eV)	Δ_{2p} (eV)[b]	$2p_{3/2}$: $2p_{1/2}$ intensity ratio[c]
$Cs_xTi_{2-x/2}Zn_{x/2}O_4$	457.7 (1.0)[d]	463.4 (1.9)	5.7	2.1:1.00
$H_{2x}Ti_{2-x/2}\square_{x/2}O_4\cdot H_2O$	458.5 (1.1)	464.2 (1.8)	5.7	2.1:1.00
	459.1 (2.0)	465.2 (2.2)	6.1	2.2:1.00

[a] Estimated experimental error ± 0.2 eV. [b] Separation between the $2p_{3/2}$ and $2p_{1/2}$ photoelectron peaks. [c] Integrated intensity according to the contribution of each peak to the total number of counts under the $2p_{3/2}$ and $2p_{1/2}$ peaks. [d] Values in brackets are the fwhm of the peaks.

the protonic titanate $H_{2x}Ti_{2-x/2}\square_{x/2}O_4\cdot H_2O$. As discussed above, the extraction of a Zn atom from the host layers will leave behind a vacant octahedral site as well as two unbonded O1 anions. Because the formation of hydroxyls and the removal of O1 species from the lattice are unlikely (e.g., Figure 7 and 10), these O1 species will have to be balanced, mostly, by the Ti atoms in the TiO_6 octahedra nearby. We therefore suggest that the Ti 2p binding energy shifts during the protonation of the $Cs_xTi_{2-x/2}Zn_{x/2}O_4$ were strongly correlated to the nature of the first coordination sphere of Ti atoms in the framework.[29]

The O 1s spectrum of the $Cs_xTi_{2-x/2}Zn_{x/2}O_4$ (Figure 12a) has its maximum at 529.2 eV, a distinct shoulder at 530.8 eV with a pronounced tail on the high energy side of the peaks. There appears to be at least three spectral contributions, of which the binding energy is 529.2 eV for 2-coordianted oxygen O1, 530.8 eV for 4-coordianted oxygen O2, and 532.3 eV for H_2O, respectively. Note that the binding energy of the 2-coordianted oxygen O1 is lower than that of the 4-coordianted oxygen O2. This is in line with the two short Ti−O1 bonds 1.845(2) Å, in comparison with the two long Ti−O2 bonds 2.162(2) Å. Upon protonation, the interlayer Cs ions are exchanged with protons in form of H_3O^+. The lattice O1 species will bond weakly with the interlayer H_3O^+ ions through hydrogen bonding, which may account for a higher binding energy of the O1 species in the $H_{2x}Ti_{2-x/2}\square_{x/2}O_4\cdot H_2O$ than that in the $Cs_xTi_{2-x/2}Zn_{x/2}O_4$ (Table 6). The binding energy for the O2 component keeps almost unchanged. Moreover, an increased H_2O content is noticed, from 7.48% of the $Cs_xTi_{2-x/2}Zn_{x/2}O_4$ to 23.13% of the $H_{2x}Ti_{2-x/2}\square_{x/2}O_4\cdot H_2O$ (Table 6), in agreement with the structural analyses (Figure 8).

The formulation $H_{2x}Ti_{2-x/2}\square_{x/2}O_4\cdot H_2O$ seems unusual because its proton content of 1.4 (for $x = 0.7$) exceeds the molar amount of water.[30] Moreover, because all exchanged protons are located in the interlayer space, the high proton content of the $H_{2x}Ti_{2-x/2}\square_{x/2}O_4\cdot H_2O$ may indicate a very complex interlayer environment that is sharply different from those seen for isomorphous compounds.[8,9,13,17,18] For example, in the $H_xTi_{2-x/4}\square_{x/4}O_4\cdot H_2O$[13,17,18] and the $H_xTi_{2-x/2}O_{4-x/2}\cdot H_2O$,[9] only 70% of the interlayer water molecules are in the form of H_3O^+ and the rest are H_2O. In this work, as suggested by the

(28) Perkins, C. L.; Henderson, M. A.; McCready, D. E.; Herman, G. S. *J. Phys. Chem. B* **2001**, *105*, 595–596.

(29) Nesbitt, H. W.; Legrand, D.; Bancroft, G. M. *Phys. Chem. Miner.* **2000**, *27*, 357–366.

(30) In ref 8, the calculated proton content of the $H_{4x/3}Ti_{2-x/3}\square_{x/3}O_4\cdot H_2O$ ($x = 0.8$) is about 1.07; the authors state an actual value around 1.1.

Table 6. O 1s Binding Energy for $Cs_xTi_{2-x/2}Zn_{x/2}O_4$ and $H_{2x}Ti_{2-x/2}\square_{x/2}O_4\cdot H_2O$

compound	O1 (eV)[a,b]	O2 (eV)	H_2O (eV)
$Cs_xTi_{2-x/2}Zn_{x/2}O_4$	529.2 (1.1)[c]	530.8 (1.7)	532.3 (1.5)
$H_{2x}Ti_{2-x/2}\square_{x/2}O_4\cdot H_2O$	529.9 (1.1)	530.7 (1.6)	532.1 (2.2)

[a] Estimated experimental error ± 0.2 eV. [b] Oxygen with different coordination numbers (e.g., Table 2). [c] Values in brackets are the fwhm of the peaks.

chemical formula $H_{2x}Ti_{2-x/2}\square_{x/2}O_4\cdot H_2O$ ($x = 0.7$), every interlayer site would be occupied by a water molecule carrying 1.4 net positive charges. Alternatively, there would be 0.4 extra proton shared by every H_3O^+ ions in every interlayer sites, implying a vigorous dynamic equilibrium of the protons in the interlayer spaces. However, the precise arrangement of these H atoms in the interlayer region is too complex to be determined with the XRD data. As shown in Figure 13a, the Raman scattering spectrum of the $H_{2x}Ti_{2-x/2}\square_{x/2}O_4\cdot H_2O$ at high wavenumber region displays several distinctive Raman bands related to the OH bending and/or stretching vibrations.[18] These spectral features are in general similar to those of the $H_xTi_{2-x/4}\square_{x/4}O_4\cdot H_2O$ (Figure 13b). However, the OH stretching vibration modes at 3270 cm^{-1} and 3390 cm^{-1} are much more prominent in the $H_{2x}Ti_{2-x/2}\square_{x/2}$-$O_4\cdot H_2O$ than those of the $H_xTi_{2-x/4}\square_{x/4}O_4\cdot H_2O$, revealing a liquidlike interlayer environment for the former in comparison with an icelike one for the later. These different interlayer environments are apparently correlated to these isomorphous compounds with different proton contents.

Amine Intercalation of $H_{2x}Ti_{2-x/2}O_4\cdot H_2O$. As a consequence of extractable Zn atoms located in the host framework, the protonic titanate $H_{2x}Ti_{2-x/2}\square_{x/2}O_4\cdot H_2O$ would have very high charge density in comparison with its isomorphous compounds.[8,9,17] Table 7 lists the structural and compositional aspects for these layered protonic titanates for comparison. Obviously, the protonic titanate H_{2x}-$Ti_{2-x/2}\square_{x/2}O_4\cdot H_2O$ is notable for its largest ion exchange capacity, largest charge density and smallest interlayer distance among all isomorphous compounds reported so far.

Usually, layered compounds with smaller charge densities and large interlayer distances imply weaker electrostatic and steric interactions between the host layers and the interlayer species, which in turn promote incorporation of interlayer guests. This has been used to understand the excellent exchange capability observed in the $H_xTi_{2-x/4}$-$\square_{x/4}O_4\cdot H_2O$[13,17] in comparison with other layered titanates such as $H_2Ti_3O_7\cdot H_2O$. As shown in Table 7, if the protonic titanate $H_{2x}Ti_{2-x/2}\square_{x/2}O_4\cdot H_2O$ would follow this charge density-exchange capability relationship, a very "dry" interlayer environment could be expect due to its extraordinarily high charge density (0.060/Å^2) as well as relatively small interlayer distance (8.97 Å) in comparison with those of the $H_xTi_{2-x/4}\square_{x/4}O_4\cdot H_2O$ (i.e., 0.031/Å^2 and 9.23 Å, respectively). This seems in contrast with the experimental findings (e.g., Figure 13). Ion exchange and intercalation behaviors of the obtained protonic titanate $H_{2x}Ti_{2-x/2}\square_{x/2}$-$O_4\cdot H_2O$ were therefore examined.

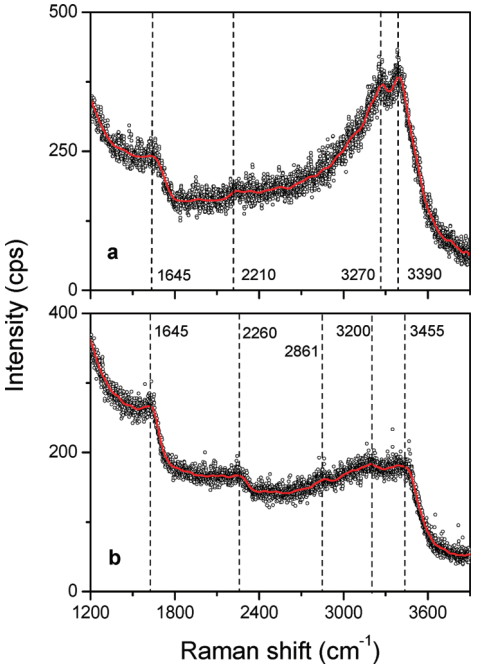

Figure 13. Raman scattering spectra of (a) $H_{2x}Ti_{2-x/2}\square_{x/2}O_4\cdot H_2O$ and (b) $H_xTi_{2-x/4}\square_{x/4}O_4\cdot H_2O$ at high wavenumbers. Curve b is shown only for comparison. Dash lines are drawn in to guide the eye. Solid lines represent the smoothed experimental data (open circles).

The protonic titanate $H_{2x}Ti_{2-x/2}\square_{x/2}O_4\cdot H_2O$ has excellent acid−base ion exchange capabilities in aqueous media to accommodate a wide variety of guests such as inorganic cations and organic bases in its interlayer spaces, similar to those observed for the $H_xTi_{2-x/4}\square_{x/4}$-$O_4\cdot H_2O$[13,17] and the $H_xTi_{2-x/4}\square_{x/4}O_4\cdot H_2O$.[8] Figure 14 displays, for example, the XRD patterns of the amine-intercalated compounds. These XRD patterns show a series of well-defined sharp basal diffraction peaks. These reflections can be indexed as (0k0), which is indicative of a lamellar structure with gallery heights dependent on the amines employed.[8,9] For example, the interlayer distance of the TBA-intercalated titanate is about 17.40 Å (Figure 14a). The increased interlayer distance of 17.40 Å compared to 8.97 Å for the original protonic titanate indicates that the TBA^+ ions have been intercalated into the interlayer regions.[13] The TMA-intercalated titanate has an interlayer distance of 16.55 Å, together with a minor phase with interlayer distance of 12.56 Å (Figure 14b); the former can be accounted for by a bilayer hydrate and the latter by a monolayer one.[8] The prominent exchange capability observed for the protonic titanate $H_{2x}Ti_{2-x/2}\square_{x/2}O_4\cdot H_2O$ indicates that the incorporation of guest species into the interlayer spaces would also be accompanied by nonquantitative intercalation reactions with driving forces other than the ion exchange, such as the hydrophobic interactions between the organic molecules. In this regard, the protonic titanate $H_{2x}Ti_{2-x/2}$-$\square_{x/2}O_4\cdot H_2O$ may represent an ideal system to understand the thermodynamic and kinetic aspects of the ion exchange reaction, especially for lepidocrocite titanates.

The intercalation of bulky amine ions results in also the swelling and delamination of the protonic titanate

Table 7. Comparison of Different Protonic Titanates with Lepidocrocite-Type Layered Structure

compd[a]	ion exchange capacity[b] (mequiv/g)	interlayer spacing (Å)	charge density[c] (Å^{-2})	ref
$H_xTi_{2-x/4}\square_{x/4}O_4\cdot H_2O$	4.12	9.23	0.031	17
$H_xTi_{2-x/2}O_{4-x/2}\cdot H_2O$	4.48	9.06	0.032	9
$H_{4x/3}Ti_{2-x/3}\square_{x/3}O_4\cdot H_2O$	5.55	9.27	0.041	8
$H_{2x}Ti_{2-x/2}\square_{x/2}O_4\cdot H_2O$	8.62	8.97	0.060	this study

[a] $x = 0.7$. [b] Calculated on the basis of chemical formula. [c] Calculated as $x/(2ac)$.

$H_{2x}Ti_{2-x/2}\square_{x/2}O_4\cdot H_2O$ into its molecular single sheets with

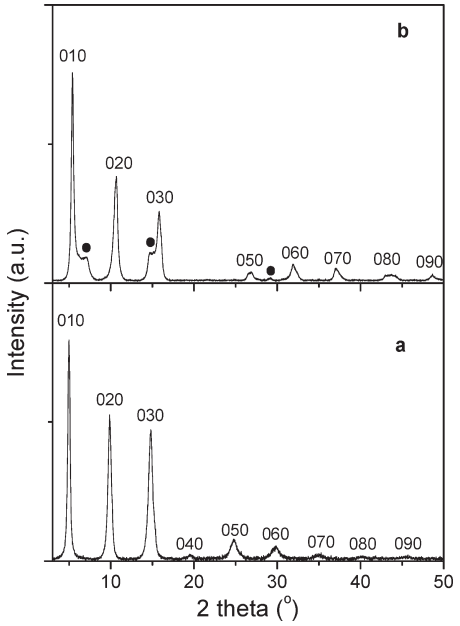

Figure 14. XRD patterns of the amine-intercalated titanates: (a) TBA-titanate and (b) TMA-titanate. Solid circles in panel b indicate a minor phase with interlayer distance of 12.65 Å.

distinctive 2D morphology, i.e., titanate nanosheets,[13] of a mean composition $Ti_{1-\delta}\square_\delta O_2^{4\delta-}$ ($\delta = 0.175$). As shown in Figure 15a, the individual exfoliated titanate nanosheets have typical platelike morphologies. The shapes and lateral sizes of delaminated nanosheets depend on the ultrasonic irradiation during the AFM sample preparation (Figure 15b). The measured thickness of the individual titanate nanosheets is around 1.4 nm, see Figure 15c. Due to the presence of linking PEI molecule between the Si substrate and the titanate nanosheets, the intrinsic thickness of the individual nanosheets is supposed to be less than 1 nm, of which, however, the exact value is difficult to obtain.

The interesting structural and physical properties of the 2D titanate nanosheets that delaminated from the $H_xTi_{2-x/4}\square_{x/4}O_4\cdot H_2O$[13,17] and/or $H_{4x/3}Ti_{2-x/3}\square_{x/3}O_4\cdot H_2O$[8] have spurred considerable interesting in the assembly of functional nanostructures,[11] such as hybrid multilayer films,[15] and microporous materials with inorganic pillars.[16] It shall be emphasized that the titanate nanosheets reported so far can be distinguished between each other by their different defect

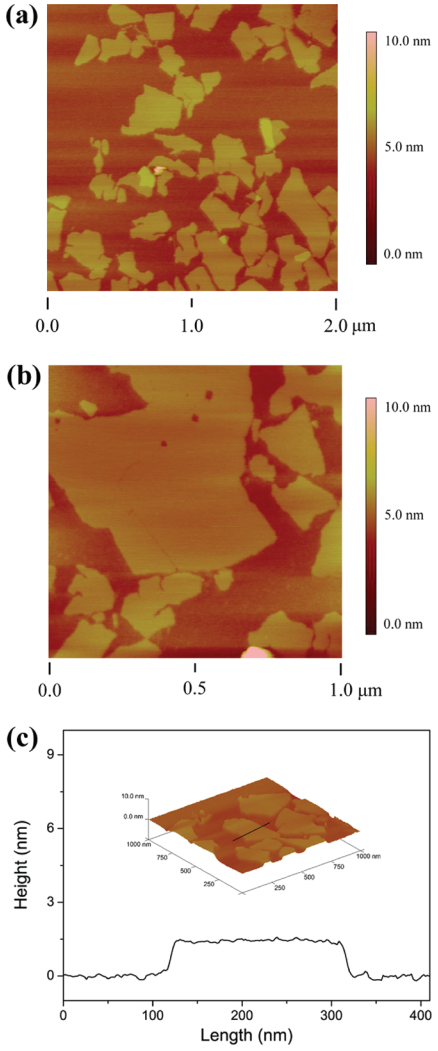

Figure 15. Tapping mode AFM images of the exfoliated titanate nanosheets (from TBA-intercalated titanate) on a PEI-coated Si wafer. Inset of panel c shows a 3D picture, where the marked region is analyzed.

contents and charge densities as given by δ in the chemical formula $Ti_{1-\delta}\square_\delta O_2^{4\delta-}$, where δ is 0.0875, 0.117, and 0.175 for those received from $H_xTi_{2-x/4}\square_{x/4}O_4\cdot H_2O$,[13,17] $H_{4x/3}Ti_{2-x/3}\square_{x/3}O_4\cdot H_2O$ (considering $x = 0.7$),[8] and $H_{2x}Ti_{2-x/2}\square_{x/2}O_4\cdot H_2O$, respectively. Because it is still not clear how the presence of cationic vacancies in the titanates and the titanate nanosheets affects their physicochemical properties,[14] the protonic titanate $H_{2x}Ti_{2-x/2}\square_{x/2}O_4\cdot H_2O$ and its molecular single sheets $Ti_{1-\delta}\square_\delta O_2^{4\delta-}$ ($\delta = 0.175$) obtained in this work will offer the possibility for a comparison study on these structurally relevant compounds.

It is worth pointings out that the $Ti_{1-\delta}\square_\delta O_2^{4\delta-}$ nanosheets may also have potentials as solid acid catalysts.[31] Domen and co-workers have demonstrated that the formation of bridging hydroxyl groups, M(OH)M′ (M = Ti, Nb, Ta; M′ = Nb, W), which are strong Brønsted acid sites

(31) (a) Takagaki, A.; Sugisawa, M.; Lu, D.; Kondo, J. N.; Hara, M.; Domen, K.; Hayashi, S. *J. Am. Chem. Soc.* **2003**, *125*, 5479–5485. (b) Takagaki, A.; Yoshida, T.; Lu, D.; Kondo, J. N.; Hara, M.; Domen, K.; Hayashi, S. *J. Phys. Chem. B* **2004**, *108*, 11549–11555. (c) Takagaki, A.; Lu, D.; Kondo, J. N.; Hara, M.; Hayashi, S.; Domen, K. *Chem. Mater.* **2005**, *17*, 2487–2489. (d) Tagusagawa, C.; Takagaki, A.; Hayashi, S.; Domen, K. *J. Phys. Chem. C* **2009**, *113*, 7831–7837.

and are intrinsic to the crystal structure of the 2D metal oxide nanosheets, is essential for the preparation of nanosheets catalysts with strong acidity.[31] Taking account of the localization of negative charge on the $Ti_{1-\delta}\square_{\delta}O_2^{4\delta-}$ nanosheets (see for example, Figure 1), it can be expected that the 2-coordinated O1 atoms shared by two nearby Ti^{4+} ions will bind to H^+, resulting in the formation of bridging hydroxyl groups, Ti(OH)Ti. Some distinctive solid acidities may be expected from the $Ti_{1-\delta}\square_{\delta}O_2^{4\delta-}$ ($\delta = 0.175$) nanosheets. This is obviously interesting and important, and worth pursuing in succeeding studies.

Conclusions

Dopant-induced defect chemistry of lepidocrocite titanates has been discussed by considering a Zn-doped phase $Cs_xTi_{2-x/2}Zn_{x/2}O_4$ ($x = 0.7$) and its protonic form $H_{2x}Ti_{2-x/2}\square_{x/2}O_4\cdot H_2O$. Some conclusions can be addressed.

The crystal structures of lepidocrocite titanate $Cs_xTi_{2-y}M_yO_4$ do not correlate strongly with the lattice dopant M. This indicates a possibility to prepare a number of titanates with intermediate compositions by modifying the lattice dopant M. It is still not easy to predict in advance the properties of lepidocrocite titanate $Cs_xTi_{2-y}M_yO_4$ with different lattice dopants; therefore a thorough analysis and characterization on every composition is required to understand the presumable dopant-dependent properties.

The Zn-doped titanate $Cs_xTi_{2-x/2}Zn_{x/2}O_4$ ($x = 0.7$) can readily be converted into its protonic form via acid exchange, during which a complete extraction of both lattice Zn atoms and interlayer Cs ions is observed. The resulted titanate $H_{2x}Ti_{2-x/2}\square_{x/2}O_4\cdot H_2O$ is notable for its high proton content, high defect content and high charge density as a consequence of exchangeable Zn atoms in the framework. A comparison among the $H_xTi_{2-x/4}\square_{x/4}O_4\cdot H_2O$, the $H_{4x/3}Ti_{2-x/3}\square_{x/3}O_4\cdot H_2O$, and the $H_{2x}Ti_{2-x/2}\square_{x/2}O_4\cdot H_2O$ will enable a better understanding on the defect chemistry and the interlayer chemistry aspects of lepidocrocite titanates. The protonic titanate $H_{2x}Ti_{2-x/2}\square_{x/2}O_4\cdot H_2O$ shows also excellent delamination reactivity to produce the 2D titanate nanosheets with mean composition $Ti_{1-\delta}\square_{\delta}O_2^{4\delta-}$ ($\delta = 0.175$). These nanosheets can be used for the assembly of artificial nanoarchitectures with intentional and controllable functionalities.

Acknowledgment. The authors acknowledge the financial assistance from the Research Council of Norway through the NANOMAT program (163565-431) and the NanoEnvironment project. T.G thanks Dr. Martin F. Sunding and Ms. Sissel Jørgensen for their help on XPS analyses. ESRF is gratefully acknowledged for beam time made available through proposal number CH-2140.